

Large-scale cortex-core structure formation in brain organoids

Ahmad Borzou¹ and J. M. Schwarz^{1,2}

¹ Department of Physics and BioInspired Institute, Syracuse University,
Syracuse, NY USA, ² Indian Creek Farm, Ithaca, NY, USA

(Dated: December 15, 2021)

Brain organoids recapitulate a number of brain properties, including neuronal diversity. However, do they recapitulate brain structure? Using a hydrodynamic description for cell nuclei as particles interacting initially via an effective, attractive force as mediated by the respective, surrounding cytoskeletons, we quantify structure development in brain organoids to determine what physical mechanism regulates the number of cortex-core structures. Regions of cell nuclei overdensity in the linear regime drive the initial seeding for cortex-core structures, which ultimately develop in the non-linear regime, as inferred by the emergent form of an effective interaction between cell nuclei and with the extracellular environment, as mediated by a dynamic cytoskeleton. Individual cortex-core structures then provide a basis upon which we build an extended version of the buckling without bending morphogenesis (BWB) model, with its proliferating cortex and constraining core, to predict foliations/folds of the cortex in the presence of a nonlinearity due to cortical cells actively regulating strain. In doing so, we obtain asymmetric foliations/folds with respect to the trough (sulci) and the crest (gyri). In addition to laying new groundwork for the design of more familiar and less familiar brain structures, the hydrodynamic description for cell nuclei during the initial stages of brain organoid development provides an intriguing quantitative connection with large-scale structure formation in the universe.

I. INTRODUCTION

What physical mechanisms are at play in determining brain structure? In humans, the beginning of brain structure begins about two weeks after fertilization with the formation of a neural plate [1]. The neural plate then folds inward on itself to form a neural tube. From this neural tube, different brain regions, such as the forebrain and the hindbrain emerge. In the forebrain, the proliferating progenitor cells in the innermost part of the tube form the ventricular zone, with extended, radial glial cells linking the cells in the ventricular zone to the outer edge of the neural tube. It is the extended radial glial cells that the inner progenitor cells crawl along to reach the outer part of the forebrain. As they do so, they differentiate to become neurons and form a cortex, consisting of six layers of cells, around 20 weeks later. In the hindbrain, the proliferation of progenitor cells occurs in the outer region with their migration towards the center of the structure. In humans, both the cerebral cortex (from the forebrain) and the cerebellar cortex (from the hindbrain) undergo shape changes in the form of folds or foliations.

Until recently, many of the biophysical models for brain structure have focused on the later stages of brain shape development, namely the development of folds of the cerebrum and the cerebellum [2–12]. These models essentially divide into two camps. The first camp consists of nonlinear elastic models with differential swelling mimicking cell growth and generating compressive forces [2, 4, 6, 8–10]. While the second camp focuses on tension-based, multi-phase models in the presence of cell growth and generating tensile forces [3, 5, 11, 12]. Experiments on ferret brains, whose folds develop *ex utero*, appear to rule out the initial version of the tension-based models by observing the displacement of brain tissue in

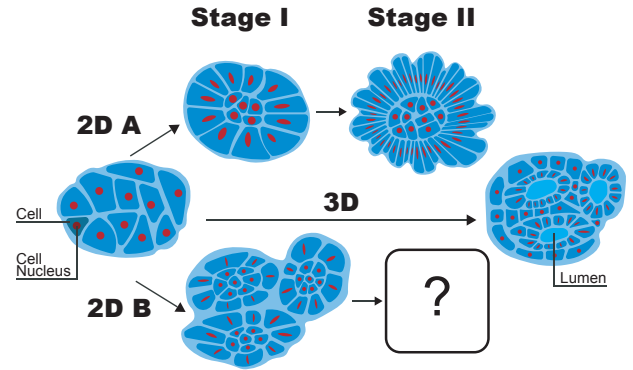


FIG. 1. A simplified version of different possible organoid shapes in quasi-2D confinement (2DA and 2DB) and not in quasi-2D confinement (3D). The cortex-core structure consists of globular-shaped cells surrounded by cells extended radially outward. One such structure emerges in the 2D A pathway during Stage I. Credit: Savana Swoger.

response to cuts in particular directions [13]. However, there exists a revised version of the initial tension-based model with a different direction of the tension that has yet to be tested experimentally [5]. Moreover, experimental studies on the developing mouse cerebellum, or the little brain, validate a new tension-based model, dubbed “buckling without bending”, and rule out a nonlinear elastic model with differential swelling [11, 12].

While many biophysical studies of brain structure focus on the folds of the cerebrum or the cerebellum, the emergence of the base structure of a cortex-core at earlier stages of development is also very important. It is this emergence that we will focus on for the first part of the manuscript using a minimal model. Interestingly, a

new *in vitro* brain system, namely brain organoids [14], provides a testing ground for understanding the emergence of brain structure [15, 16], as well as recapitulate such phenomena as neuronal diversity [17] and neuronal firing patterns [18]. One such study focuses on quasi-two-dimensional brain organoids that start as a relatively isotropic clump of cells, which is then inserted between two “plates” separated by approximately $150\ \mu\text{m}$ [16]. Within several days, the clump morphs into several substructures each with a core with globular, polyhedral-shaped cells and radially-stretched cells surrounding each core to form a cortex, or, there is only one cortex-core structure. See Fig. 1 in which latter result is labelled pathway “2D A” and the former, “2D B”. After this initial shape change in the “2D A” pathway and the cortex-core structure continues to grow, a foliation amongst the radially-stretched cells emerges. It is for this latter foliation stage that the researchers develop a theory, which is rooted in elasticity theory [16].

Here, we will first take a step back from cortex foliation and address how is it that at times multiple cortex-core structures emerge, while in other cases, just one cortex-core structure emerges. Answering this question will give us insight into cortex-core formation. Then, we will characterize the foliation of the cortex with the “buckling without bending” morphogenesis (BWBM) model since it is already able to quantitatively capture cortical foliation in blebbistatin-treated brain organoids [11]. One, therefore, wonders whether or not such an approach is applicable in the untreated case.

To explore how brain organoids acquire their cortex-core structure, which we dub Stage I, *and* subsequent cortex foliation, or Stage II (see Fig. 1), we build continuum models for each respective stage. We do so since once the cortex-core structure forms, that structure provides the basis for coarse-graining at a different scale to arrive at an extension of the BWBM model. As for Stage I, many cellular aggregates often demonstrate fluid-like behavior [19, 20], though viscoelasticity is also observed [21]. Given the cellular fluid-like behavior, an appropriate model falls under the hydrodynamics domain. At this point, it is tempting to go to a more detailed cellular-based model. However, we will take a less-detailed approach since it is not entirely clear if we can address the one versus many cortex-core structures within a detailed computational model at the outset, given the limitation of finite size.

Therefore, we seek a more minimal approach in which cell nuclei are particles. The cell nuclei interact with other cell nuclei *indirectly* via the surrounding active cytoplasm of, say, two cells, interacting with each other via their cortical tension, which ultimately drives the cell-cell interaction. Cell nuclei also interact indirectly with their extracellular surroundings. In other words, there is an *effective, active force* on cell nuclei due to cell-cell interactions an *effective, active force* on cell nuclei due to the extracellular environment. Specifically, since cell nuclei are observed to move toward each other during what is called

the linear regime, we will assume that there is an initial, effective, short-range attraction between cell nuclei. As the organoid evolves, given the dynamic and mechanosensitive nature of the active, cytoskeleton generating forces, we use several observations from experiments to determine the emergent form of the effective, active force on cell nuclei due to cell-cell and cell-environment interactions during the non-linear regime. From the emergent form of the effective, active force we will infer cortex-core structures. We will use hydrodynamic equations to describe both regimes, which will correspond to a linear regime and a non-linear regime.

Intriguingly, this vantage point draws parallels with cosmological models of large-scale structure formation in our universe at the quantitative level. Both have the same dynamical equation for the single-particle distribution function. Moreover, the initial and final states of both systems are very similar; both systems start from an initially uniform number density of particles and end in spherical shape structures. This is despite the differences such as different types of interactions, as well as the presence of growth, dissipation, and noise, for example, for living matter.

Once cortex-core structures emerge, such individual structures provide the basis for the BWBM model in which cellular growth plays a key role. The BWBM model consists of an incompressible core with a growing cortex and several other mechanical aspects of the brain organoid structure, namely, the mechanics of the surrounding Matrigel and cortical cells under tension. An initial, linear version of the BWBM model provided a physical basis for the unusual cortical thickness variations in blebbistatin-treated brain organoids—variations that cannot be readily explained by a purely elastic model. In addition, the foliations were more scalloped, or more asymmetric, in the blebbistatin-treated case as compared to the untreated case, and so a linear BWBM model, with its symmetric foliations was reasonable. Indeed, blebbistatin inhibits myosin-II, and so the intra-cellular tension in cells making up both the cortex and the core decreases [16]. At higher tensions, nonlinearities in tension are more likely to become relevant, which is what we explore here. For context, recent work has been done to take into account nonlinearity in tension in radial glial cells in the developing cerebellum [22], which are not present in the confined brain organoids at relevant time scales. We will explore a different form of nonlinearity here.

This paper is organized as follows. In Section II, we uncover a physical mechanism for cortex-core structure formation (Stage I). In Section III, we quantify how foliations/folds in the cortex emerge. We conclude with implications of our findings in Section IV.

II. STAGE I MODEL

Assuming that the brain organoid begins as an aggregate of fluid-like cells, let us begin with the dynamical equation for the one-body distribution function for cell nuclei given by

$$\frac{df}{dt} = \frac{\partial f}{\partial t} + \frac{\partial f}{\partial x^i} v^i + \frac{\partial f}{\partial v^i} \dot{x}^i = C, \quad (1)$$

where C incorporates dissipation, cell division, and fluctuations [23]. We treat the interaction between cell nuclei as mediated by the surrounding cytoskeletons associated with two attached cells, for instance, as an effective force on a cell nucleus. A surrounding cytoskeleton interacting with the extracellular environment also leads to an effective force on cell nuclei. In other words, even though nuclei do not interact directly, they interact indirectly via their respective, surrounding cytoskeletons, so using Newton's second law, the sum of the forces on the nuclei are such that the net force on them may be nonzero should they go from not moving to moving, for example.

As for how the effective force between cell nuclei is generated, a significant player is the contractile nature of the actomyosin cortex with cells fusing when in a fluid phase [24, 25]. This phenomenon points to an effective, attractive interaction between cell nuclei that is short range in the sense that the interaction involves cells in contact. There are also effective interactions between the cell nuclei and their passive environment as mediated by the cell cytoskeleton [26]. Therefore, we approximate both cell-cell and cell-environment interactions as an effective force such that \dot{x}^i in Eq. (1) refers to the effective force on cell nuclei as mediated by the cell cytoskeleton accounting for factors such as actomyosin contractility and the surrounding environment.

With this construction, there is a quantitative link with cosmology. In cosmology, to study large-scale structure formation, one constructs a dynamical equation for the time evolution of matter as encoded by the one-body distribution function, f , in the six-dimensional phase space of positions and velocities. See, for example, the Boltzmann equation [27] and the Jeans equation [28]. In the Jeans equation in cosmology, $\ddot{x}^i = g^i$, where g^i denotes gravitational acceleration [28].

Inspired by this mathematical link to cosmology, we split Stage I into linear and non-linear eras. Since cell nuclei densities are low initially, Eq. (1) is linear. We will show that the magnitude and the form of the effective force do not change the resulting structures' shape. As soon as cell nuclei densities increase, the equation becomes non-linear and the exact form of the effective force becomes relevant. We will assume that the form of the effective force can change with time as it is generated by a dynamic cytoskeleton. Given certain observations from experiments in the non-linear era, we will extract the effective force from Eq. (1). The spatial patterning of cell nuclei then emerges from the combination of (i) a robust evolution equation and (ii) observation, and is

rooted in the effective force that we derive. Specifically, we show that at the beginning of the non-linear era, the effective force between cell nuclei is attractive. However, toward the end of Stage I, the effective force changes in nature and becomes almost neutral at the center and repulsive beyond some characteristic radius of the spherical structures.

Let us now work towards a solution for Eq. (1). Since cell nuclei are roughly round shape in Stage I of brain organoid formation, we neglect their inherent structure and assumed that phase-space consists of positions and velocities only. Solving Eq. (1) analytically can be challenging. The more conventional approach is to solve its first two moments of velocities leading to two differential equations coupling the number density $\rho \equiv \int dv f$, the bulk velocity $\bar{v}^j \equiv \frac{1}{\rho} \int dv v^j f$, and $\bar{v}\bar{v}^{ij} \equiv \frac{1}{\rho} \int dv v^i v^j f$. To proceed further, one can write a third differential equation for $\bar{v}\bar{v}^{ij}$, which depends on higher moments of f . Instead, we apply a data-driven hydrodynamics approach to find a relationship between ρ and pressure for the cell nuclei [23]. To do so, we define the stress tensor as $\sigma^{2ij} \equiv \bar{v}\bar{v}^{ij} - \bar{v}^i \bar{v}^j$ and assume it is isotropic during the initial stages such that $\sigma^{2ij} = \sigma^2 \delta^{ij}$. From the observations reported in Ref.[16], we find that the pressure of the cell nuclei linearly depends on the number density with a proportionality coefficient of $\sigma^2 = 0.1$ (see Appendix A). Therefore, the final form of the evolution equation set reads

$$\begin{aligned} \partial_t \rho + \partial_i (\rho \bar{v}_i) &= C_0, \\ \partial_i \bar{v}_j + \sigma^2 \partial_j \rho + \bar{v}_i \partial_i \bar{v}_j + g_j &= \frac{1}{\rho} (C_j - \bar{v}_j C_0), \end{aligned} \quad (2)$$

where $C_0 \equiv \int dv C$ accounts for cell division and the noise, and $C_j \equiv \int dv C v_j$ accounts for dissipation and noise. Since the number density experiences minimal growth in the first 3 days of the experiment until the cortex-core structures are first observed [16], we assume C_0 only accounts for the noise. We also assume that the noise terms obey

$$\langle C_{0\text{noise}} \rangle = \langle C_{j\text{noise}} \rangle = 0, \quad (3)$$

with

$$\begin{aligned} \langle C_{0\text{noise}}(t, \vec{x}) C_{0\text{noise}}(t', \vec{x}') \rangle &= \theta \delta(t - t') \delta^3(\vec{x} - \vec{x}'), \\ \langle C_{i\text{noise}}(t, \vec{x}) C_{j\text{noise}}(t', \vec{x}') \rangle &= \gamma \delta_{ij} \delta(t - t') \delta^3(\vec{x} - \vec{x}'), \end{aligned} \quad (4)$$

where θ and γ determine the strength of each type of noise. For effects of dissipation, see Appendix A.

Given the coupled, non-linear equations above, we will divide the brain organoid evolution into linear and non-linear regimes by solving the linearized form to find the initial conditions for the non-linear evolution. However, in the non-linear regime, instead of deriving density growth in terms of the forces, we use the exact form of the differential equations, and the observations, to derive the evolution of the effective forces on the cell nuclei as they may change over time, unlike in cosmology.

A. Stage I linear regime

We assume that the number density is initially homogeneous with some small fluctuations, or $\rho \equiv \rho_0 + \delta\rho$, with $\delta\rho \ll \rho_0$. Inserting this ansatz into Eq. (2), neglecting higher order terms, and Fourier transforming, we find

$$\delta\rho(t, \vec{x}) = \int d^3k e^{i\vec{k}\cdot\vec{x}} \tilde{\delta}(t, \vec{k}), \quad (5)$$

with

$$\tilde{\delta}(t, \vec{k}) = \tilde{\delta}(t=0, \vec{k}) \cosh\left(\sqrt{\rho_0(\mathcal{L}^{-1} - \sigma^2)} kt\right), \quad (6)$$

where the Fourier transform of g_j is assumed to have the following general form $\tilde{g}_j = -ik_j \mathcal{L}^{-1} \tilde{\delta}$. In a conservative system with long-range gravitational forces, $\mathcal{L}^{-1} = k^{-2}$. For brain organoids, the forces are short-ranged and non-conservative, so \mathcal{L}^{-1} takes a more complex form. Nevertheless, the result is not sensitive to the detailed form of the attractive force in the linear regime since only the first term of its Taylor expansion contributes to the results. We assume two generic forms below.

To model the very initial overdensities, we assume that at $t = 0$ there exist N point-like random fluctuations in the density such that

$$\delta\rho(t=0, \vec{x}) = \sum_{i=1}^N c_i e^{-|\vec{x} - \vec{r}_i|^2}, \quad (7)$$

where \vec{r}_i and c_i are random and denoting the location and magnitude of each density fluctuation. All magnitudes satisfy $|c_i| \ll \rho_0$. Therefore,

$$\tilde{\delta}(t=0, \vec{k}) = \pi^{\frac{3}{2}} \sum_{i=1}^N c_i e^{-i\vec{k}\cdot\vec{r}_i} e^{-k^2/4}. \quad (8)$$

Inserting all terms back into Eq. (5), the final solution for the time-evolved number density in the linear regime reads

$$\begin{aligned} \delta\rho(t, \vec{x}) &= \frac{1}{2\pi^{\frac{1}{2}}} \sum_{i=1}^N \frac{c_i}{|\vec{x} - \vec{r}_i|} \int_0^\infty k \sin(k|\vec{x} - \vec{r}_i|) e^{-k^2/4} \\ &\times \cosh\left(\sqrt{\rho_0(\mathcal{L}^{-1} - \sigma^2)} kt\right) dk. \end{aligned} \quad (9)$$

While we do not know the exact form of the initial, effective force between cell nuclei, from observation, it is effectively short-range and contractile. So we write \mathcal{L}^{-1} in the following general form

$$\mathcal{L}^{-1} = \sum_{n=1}^{\infty} \frac{l_n}{k^{2n} + b_n^{2n}}, \quad (10)$$

where b_n^{-1} is an effective distance beyond which the force is zero. While the final over/under-densities slightly depend on the significant terms in \mathcal{L}^{-1} , as far as the effective interactions are attractive, the structures grow with a rather similar form.

In the following, we initially work with the first term of the sum in Eq. (10) and derive the final densities. Later, we repeat the same calculation with an additional term in the sum to look for sensitivity in the form of the effective force. After retaining the first term in the expansion of \mathcal{L}^{-1} , we insert the randomly generated c_i and \vec{r}_i and integral numerically for every \vec{x} over a finite area in the $x-y$ plane to determine how $\delta\rho(x, y)$ changes in time. We choose $\rho_0 = 1$, $a = 0.1$, and $b = 0.1$ to carry out the calculation. The density evolution for different time points is plotted in Fig. 2. Small over-density and under-density regions grow under the contractile forces of the cells and create cortex-core seeds for the non-linear regime. We also have repeated the calculations for \mathcal{L}^{-1} containing the first *two* terms in eq. (10). The final density is presented in Fig. A2, indicating that, as long as the effective force between nuclei is attractive, the larger-scale density structures grow with a rather similar form. The difference is more in the timing of the growth. The stronger the force, the faster the structures form. The reason for the similar spatial structure is that regardless of the exact form of the force, in the linear era, one can always perform a Taylor expansion and neglect the higher order terms. Hence, the effective force always enters the equations with the same form regardless of its exact form.

B. Stage I non-linear regime

At the end of the linear era, the cell nuclei around each existing over-dense region start to migrate toward a center. However, unlike in the linear regime, results may indeed depend on the details of the net, effective force on cell nuclei. Given the dynamic nature of the cytoskeleton mediating the effective force, combined with the existence of experimental data, we adjust our approach and use a data-driven approach to derive the effective force on nuclei using our knowledge of density evolution from observations. Our prediction for the emergent, effective force can be tested with additional experiments.

We now focus on one of the over-dense centers and assume a spherical symmetric structure with $\rho \simeq \rho_0$, $\partial_t \rho \simeq 0$, $\bar{v}_r = -v_0$ and reset time to $t = 0$. The evolution equations now become

$$\begin{aligned} \frac{\partial \rho}{\partial t} + \frac{2}{r} \rho \bar{v}_r + \partial_r(\rho \bar{v}_r) &= C_0, \\ \frac{\partial}{\partial t} \bar{v}_r + \sigma^2 \partial_r \rho + \bar{v}_r \partial_r \bar{v}_r + g_r &= \frac{1}{\rho} C_r, \end{aligned} \quad (11)$$

where we have used the isotropic assumption to infer that in the spherical coordinate system $\vec{v} = (\bar{v}_r, 0)$.

We use the first equation to solve for the bulk velocity in terms of the number density and then make the following assumptions for the final state of what becomes the cortex-core structure: $\rho \rightarrow F(r)$, where $F(r)$ is the form of the number density observed around Day 3 of the experiment (see Fig. A3), and $\bar{v}_r \rightarrow 0$. Given the initial and final conditions, we construct an analytic form for

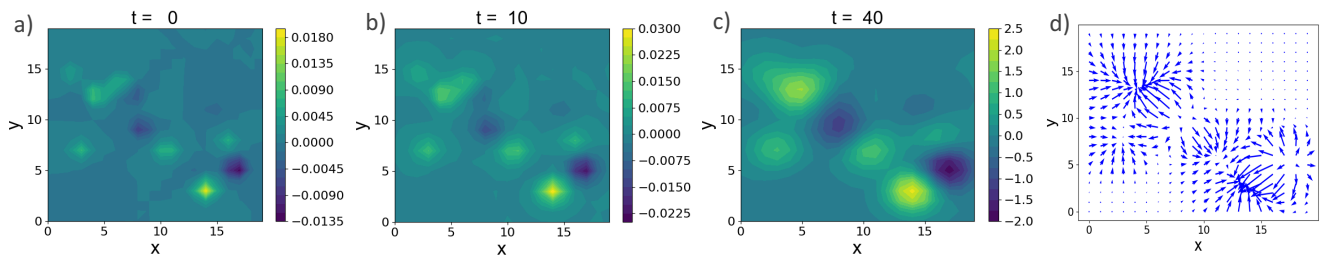


FIG. 2. a-c): The time evolution of $\delta\rho$ for $\mathcal{L}^{-1} = \frac{1}{k^2+0.1^2}$ with $\rho_0 = 1$, $a = 0.1$, and $b = 0.1$. d): The corresponding force field at $t = 40$.

$\rho(t, r)$ so that we can ultimately determine the interaction between the cell nuclei. Unlike in the linear regime (and in cosmology), the interactions between cell nuclei can change to the cytoskeletal restructuring in response to interactions with other cells and/or with the environment. Hence, $g_r(t, r)$ is unknown as are the damping effects in $C_r(t, r)$,

With these assumptions, the time evolution for $\bar{v}_r(t, r)$ and $g_r(t, r) - C_r(t, r)/\rho(t, r)$ can be determined. See the appendix for details. The results for the latter are shown in Fig. 3. The bulk velocity is initially position-independent and toward the center. Over time, it becomes a position-dependent function and evolves toward zero. The net force is toward the center of the core initially, but changes nature over time and becomes position-dependent. By Day 3, near the edge, the net force is outward, indicating that the nuclei are being indirectly pulled on by the extracellular environment, i.e. the cell cytoskeleton has developed subcellular structures to attach to the extracellular environment. We have not assumed the existence of such an effect but derived it based on data and the theoretical framework. Experiments can measure this net force via laser ablation.

Subtracting from the net force the assumed short-range, attractive interaction between cell-nuclei invoked in the linear regime, we find a new effective force that emerges during the non-linear regime. See Fig. 3. This emergent force is attractive close to the center and repulsive around the edge. Since it is attractive near the center, the density of cell nuclei is higher than near the edge. Where the emergent net force on cell nuclei goes from attractive to repulsive is where we anticipate the boundary of the cortex-core to be. If one were to invoke a Voronoi tessellation of the cell nuclei to obtain cell shapes [29, 30], then the cell shapes across this boundary would be elongated radially. Given our continuum analysis, we cannot determine whether or not the cortex is one cell layer thick or many cell layers thick. Should the cortex be many cell layers thick, then the cells farther away from the boundary will not necessarily be elongated. In any event, it turns out that the cortex is one cell layer thick, approximately. The mechanism for this phenomenon must be explored with a more detailed, cellular-based model. With a Voronoi tessellation, the positions of the cell nuclei are the positions of the center of mass of a deformable cell nu-

clei. If cells are elongated just beyond the zero-net force boundary, then cell nuclei are as well since cell nuclei shape reflect cell shape [31]. We, thus, infer the formation of a cortex-core structure, though, again, the overall thickness of the cortex has yet to be determined. We use the term “large-scale” to denote that it is a multicellular structure. In the case of multiple cortex-core structures, supracellular actomyosin cabling [32] may act as an “external” environment such that multiple cortex-core structure can form simultaneously. Finally, for both the linear and non-linear regimes, the cell nuclei densities were not large enough to worry about overlaps between cell nuclei, or even shorter-range repulsive interactions.

III. FOLIATION FORMATION VIA A NONLINEAR BUCKLING WITHOUT BENDING MODEL

Now that cortex-core structures form, we proceed to the subsequent foliation of the cortex observed in the “2D A” pathway. To do so, we turn to the BWBM model, which is a coarse-grained, continuum model at a larger scale to accommodate the predominance of cell growth at this stage. The initial version of the BWBM model assumes a cortex-core structure and has demonstrated qualitative agreement with the foliation found in the quasi-two-dimensional brain organoids in pathway “2D A” with the addition of blebbistatin [11]. A new nonlinearity, as we will show, extends the applicability of the model to the untreated case.

More precisely, we model the growing cortex-core structure as a two-dimensional annulus-like region having outer radius r and thickness t , which are scalar functions of an angular coordinate θ such that t is measured in the radial direction (see Fig. 4). We also assume that r and t are single-valued, i.e., no overhangs. We then introduce the quasi-static, coarse-grained energy functional

$$E[r, t, \frac{dt}{d\theta}] = \int d\theta \left\{ k_r (r - r_0)^2 - k_t (t - t_0)^2 + \beta (1 + \lambda t) \left(\frac{dt}{d\theta} \right)^2 \right\}, \quad (12)$$

to be minimized subject to a constraint on the area of the core, i.e., $\frac{1}{2} \int d\theta (r - t)^2 = A_0 = \text{constant}$. The variational problem then becomes $\delta \left(E - \mu \int d\theta (r - t)^2 \right) = 0$, where

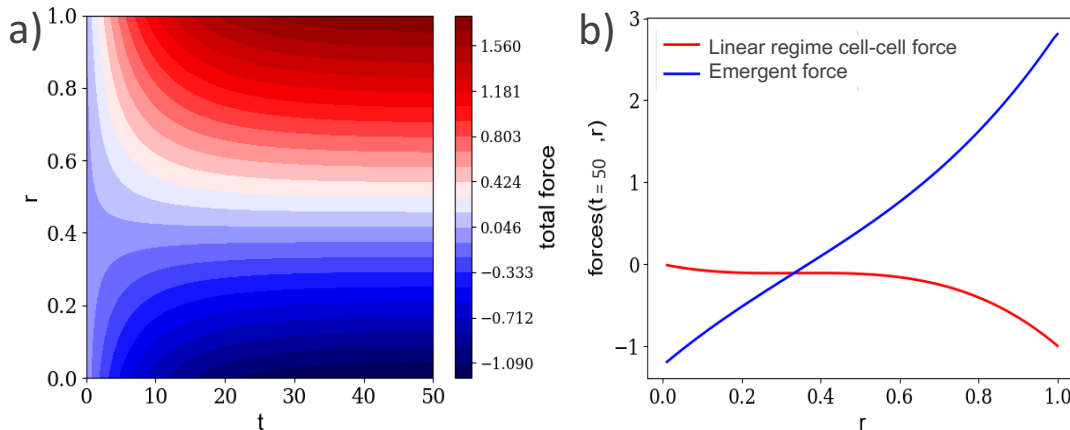


FIG. 3. a) The time evolution of the net force on the cell nuclei as a function of the radius of one cortex-core structure. b) The emergent net force on cell nuclei at the final time and the initial net, attractive force between two cell nuclei used in the linear regime, both as functions of the radius of one cortex-core structure.

μ is a Lagrange multiplier.

Shape change as a function of time, here, is encoded in changes in the constants at hand. Addressing Eq. 12, k_r , k_t , and β are all positive constants. The first term encodes a preferred radius r_0 , which we assume to be constant. This preferred shape represents the energy cost in deforming the Matrigel, or the extracellular environment. The second term favors thickening of the cortex with respect to a reference thickness t_0 , which we also assume to be constant, given its negative contribution. Thus, while k_r is a modulus, k_t can be regarded as a “growth potential” in the form of an anti-harmonic term. Therefore, the validity domain of this analysis is only limited to those cases in which the thicknesses are small, i.e., the energy functional is bounded.

The corresponding terms compete with one another due to the incompressibility of the core, thereby driving the system away from its preferred shape. The third term penalizes spatial variations in thickness with the nonlinear λ contribution representing the active, adaptive contractile nature of the cells. As cortex cells are extended/elongated, they build cytoskeletal structures to adapt to the extension with the development of stress fibers, for example, to regulate their strain and, therefore, resist the extension [33]. The addition of blebbistatin prevents such structures from resisting the extension, therefore, denoting the $\lambda = 0$ case. We note that another form of nonlinearity has been studied in the context of nonlinear elasticity of the radial glial cells spanning the cerebellum [22]. Here, there are no such radial glial cells, at least during these early stages.

Assuming the initial cortex-core shape to be a circle with radius r_0 , the Euler-Lagrange equations result in an unconventionally driven, nonlinear oscillator equation. Specifically, the Euler-Lagrange equation for $t(\theta)$ is of the

form

$$(1 + \lambda t) \frac{d^2 t}{d\theta^2} + q^2 t = -\frac{1}{2} \lambda \left(\frac{dt}{d\theta} \right)^2 + B, \quad (13)$$

with $q^2 = \frac{k_t}{\beta} \left[1 + \frac{\epsilon c}{(1-\epsilon)} \right]$ and $B = \frac{k_t}{\beta} \left[t_0 + \frac{\epsilon c r_0}{(1-\epsilon)} \right]$ after defining $\epsilon = \frac{\mu}{k_r}$ and $c = \frac{k_r}{k_t}$. In addition, there is a linear relationship between t and r , i.e., $r = \frac{-\epsilon t + r_0}{1-\epsilon}$. We can, therefore, numerically solve for the shape of the cortex-core structure as a function of the parameters. The RK45 method of the `scipy.integrate` package in Python is used for the numerical integration of the above nonlinear differential equation. Note that we treat the t -dependent mass term perturbatively given the existence of the usual, mass term.

The results for the subsequent brain organoid evolution are plotted in Fig. 4 for different k_r s, which decreases with time as the Matrigel softens due to compression [34]. We observe for the nonlinear case an asymmetry developing between the crest (the gyri) and the trough (the sulci) to approach a more scalloped form prominent in the untreated brain organoids. To more clearly demonstrate the differences between the linear BWBM model and this nonlinear version, we present shapes for both cases in Fig. 5. On the other hand, the scallops are not as packed tightly together as observed in the experiments. Interestingly, a recent nonlinear extension of the BWBM model also demonstrated more scalloped foliation with a nonlinearity introduced in k_r to account for the nonlinear elasticity of the radial glial cells [22]. Another interesting feature of the BWBM model is that once the first generation of foliations/folds appear, we anticipate the potential for subsequent generations to occur as the boundaries of the first generation foliation create a sub-system within the overall structure such that foliation process can occur within the sub-system, given the number of foliations is essentially scale-invariant [11, 22, 35]. In fact, this type of higher-order branching process is

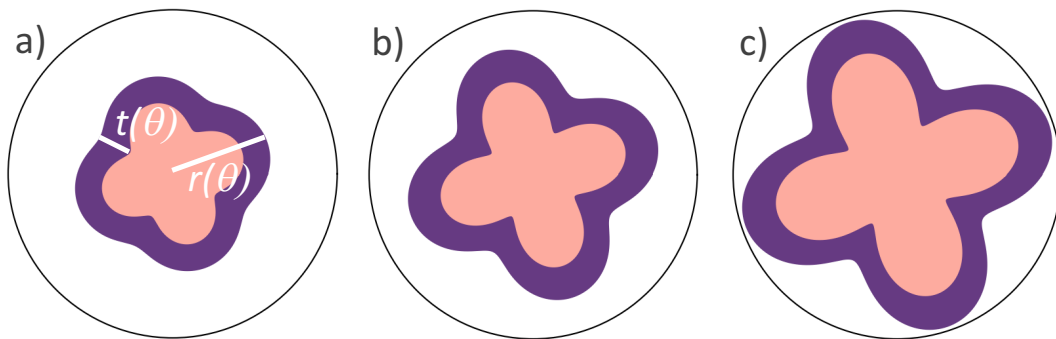


FIG. 4. BWBM model for the foliation of wild-type brain organoids pathway 2D A as time increases to the right. Parameters used are $k_t/\beta = 15.6$, $t_0/r_0 = 0.7$, $\lambda/r_0 = 25$ for a)-c) and for a) $\mu/k_r = 0.72$, $k_r/k_t = 0.043$, for b) $\mu/k_r = 0.855$, $k_r/k_t = 0.036$, for c) $\mu/k_r = 0.9$, $k_r/k_t = 0.034$.

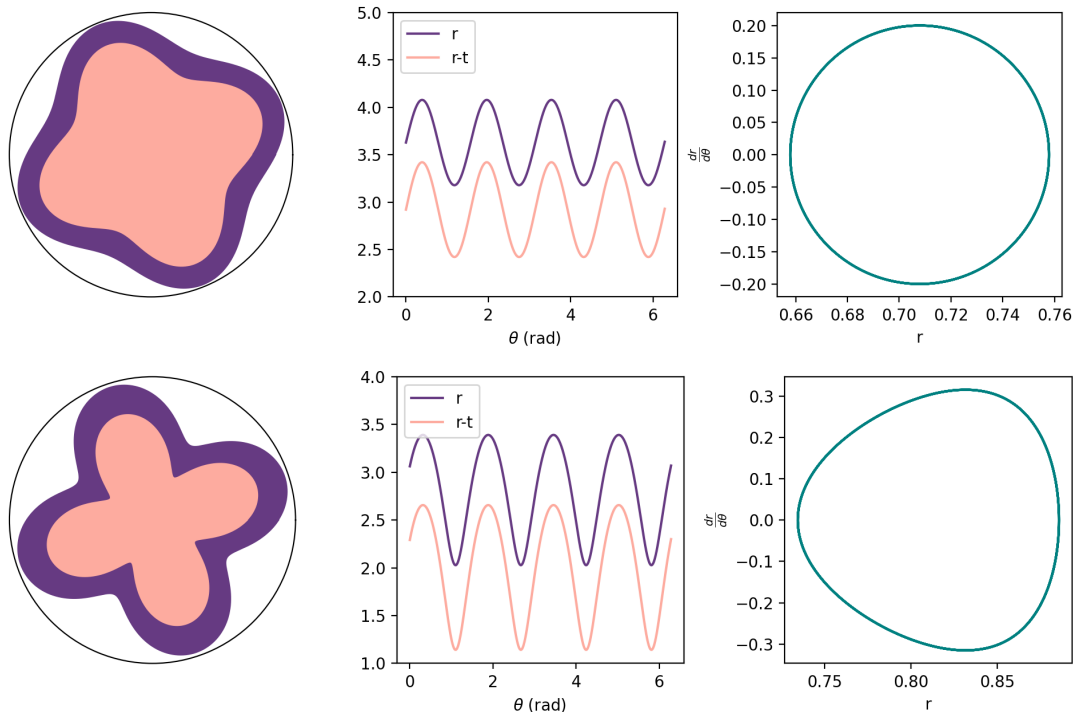


FIG. 5. Top row: Results for the linear version of the BWBM model, or $\lambda/r_0 = 0$, with other parameters the same as in Fig. 4c. Bottom row: Results for the nonlinear version of the BWBM model with $\lambda/r_0 = 25$ for the first term in the perturbation expansion for the t -dependent mass term and with other parameters the same as in Fig. 4c.

observed in brain organoid experiments [16] and in the developing, approximately cylindrical cerebellum [36].

IV. DISCUSSION

We have established a two-part framework to quantify the shape of brain organoids as they develop. Both parts are rooted in the assumption that the material is not purely elastic. Indeed, tissue fluidity has emerged as a driver of shape change in animal development more generally [37, 38]. The first part of the framework mod-

els the interactions between cell nuclei due to activity to examine how multiple, large-scale core-cortex structures emerge in the confined case. If we know the initial density map of cell nuclei, we can predict the number and size of the cortex-core structures. We can also predict the subsequent foliation of an individual cortex-core structure. Predictions for foliation in multiple cortex-core structures require a more detailed analysis of an interacting version of the BWBM model.

While Stage II of the “2D B” pathway was reported in the literature [16], it is not clear if such multi-core-cortex structures exhibit Stage II behavior. Considering just

two-core-cortex structures with a very small interface in between initially, then each cortex-core structure evolves independently of each other until the interface increases due to the growth. Earlier work has shown that the linear BWBM model in the presence of a confining wall flattens the scallops [22]. Treating each structure as a confining presence of the other, will thus, flatten the scallops and so one may observe some foliation with different shapes along the interface between the two structures as compared to the interface with Matrigel. However, should the interface between the two structures not be small to begin with, then one must also treat the two core-cortex structures as a coupled system with the spherical symmetry now broken. We are currently extending the BWBM model to describe multiple-cortex-core structures with interfaces in between, suggesting that the extent of the foliation will depend on such details as the difference in growth potentials between the two structures, etc.

While we have focused here on the structure of quasi-two-dimensional brain organoids, three-dimensional brain organoid shapes typically consist of multiple large-scale structures [14]. These large-scale, or multi-cellular structures are cortex-lumen structures embedded within non-cortical/non-extended cells. Our framework for Stage I applies under these conditions as well. Variations in cell nuclear density, as well as variations in contractility of the cells, determine where the large-scale structures emerge. Regions, where the cellular contractility is less than the average, translate to cellular material effectively acting as a passive, or extracellular, environment. The regions of underdensity, as before, translate to an effective repulsive force to push cells apart. The more the cells move apart, the more likely ruptures will occur at the cell-cell interface to create a lumen or hole. The shape of such holes depends on the shape of the regions of less active cells to which the more active cells are pulled towards. Predicting the detailed shape of these large-scale structures, therefore, requires some modeling at the cell-cell interface level to pinpoint the rupture locations, which we do not address here. Recent work interpolating between confluent and non-confluent tissue, thereby identifying points of rupture, may help [39]. In the confined case, perhaps stronger interaction with the passive environment prevents such rupture. However, our work suggests that a very homogenous organoid with an un-

derdensity region in the center of a spherical organoid leads to one cortex-lumen structure embedded in a sea of cells. See Fig. 6.

If we are to understand how the brain attains its shape, brain organoids serve as an excellent *in vitro* platform. While brain organoids do *not* currently mimic brain shape, one can now design conditions in which higher-order foliations/folds are more likely to occur in the confined case to more closely resemble the cerebellum. Moreover, a three-dimensional brain organoid with one cortex-lumen structure can potentially be engineered in which the cortex is layered by the addition of cells at the cell-cell rupture site in such a way that they also become extended. Therefore, one can create more similar shapes to the mammalian brain or even less similar to study how brain shape affects brain function. For instance, the honeybee brain has a rather different structure than a mammalian brain [40]. Moreover, at the heart of subsequent brain development is the existence of elongated cells that serve as a backbone for the initiation of neurons, cells unique to the central nervous system, which, therefore, requires more modeling attention.

Finally, the framework we use to quantify large-scale structure formation in brain organoids for Stage I is the same as the hydrodynamic framework for large-scale structure formation in the universe. In the early universe, quantum fluctuations induce negligible mass overdensities that grow over time, by attracting nearby mass, to ultimately form galaxies [41–43]. Otherwise, despite the attractive nature of gravity, an exactly uniform universe will stay uniform forever. Given this mathematical correspondence, perhaps studying multi-cellular structure formation in a petri dish with living matter may tell us something intriguing about the potential for engineering new types of mini-universes, i.e., large-scale structure formation in these new kinds of universes and morphogenesis are inextricably linked.

ACKNOWLEDGMENTS

JMS acknowledges Mahesh Gandikota and Orly Reiner for discussions and financial support from grant NSF-DMR-1832002 and an Isaac Newton Award from the DoD.

-
- [1] D. H. Sanes, T. A. Reh, and W. A. Harris, *Development of the Nervous System* (Academic Press, 2012).
 - [2] D. P. Richman, R. M. Stewart, J. W. Hutchinson, and V. S. Caviness, Mechanical model of brain convolitional development, *Science* **189**, 18 (1975).
 - [3] D. C. Van Essen, A tension-based theory of morphogenesis and compact wiring in the central nervous system, *Nature* **385**, 313 (1997).
 - [4] P. Bayly, R. Okamoto, G. Xu, Y. Shi, and L. Taber, A cortical folding model incorporating stress-dependent growth explains gyral wavelengths and stress patterns in the developing brain, *Physical Biology* **10**, 016005 (2013).
 - [5] O. V. Manyuhina, D. Mayett, and J. M. Schwarz, Elastic instabilities in a layered cerebral cortex: a revised axonal tension model for cortex folding, *New Journal of Physics* **16**, 123058 (2014).
 - [6] S. Budday, P. Steinmann III, and E. Kuhl, Physical biology of human brain development, *Frontiers in Cellular Neuroscience* **9**, 257 (2015).
 - [7] B. Mota and S. Herculano-Houzel, Cortical folding scales

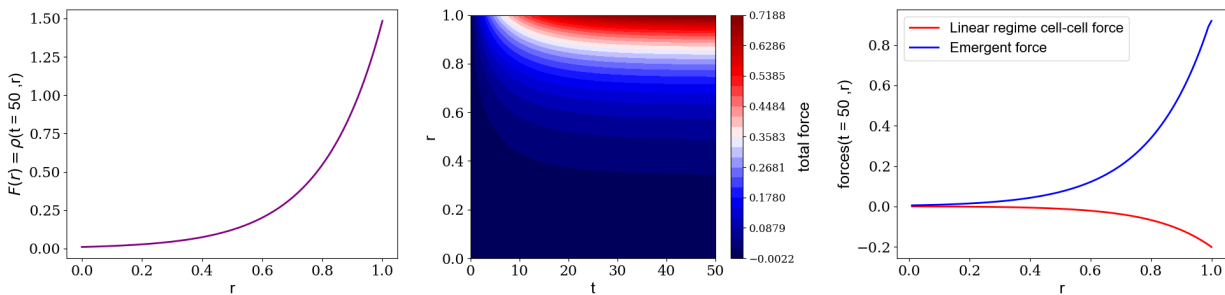


FIG. 6. In three dimensions, brain organoids have a hole, or lumen, at the center of large-scale/multi-cellular structure and the cell nuclei are all in the outer cortex region. (Left): The number density of cell nuclei at the end of the nonlinear era, assuming a hole in the center of the cortex-lumen structure (Middle): The time evolution of the net force on cell nuclei for a cortex-lumen structure. (Right): The initial, net attractive force on cell nuclei (red) due to cell-cell interactions and the emergent, net force (blue) as the cytoskeleton restructures itself, using the assumed cell nuclei number density.

universally with surface area and thickness, not number of neurons, *Science* **349**, 74 (2015).

- [8] T. Tallinen, J. Y. Chung, F. Rousseau, N. Girard, J. Lefèvre, and L. Mahadevan, On the growth and form of cortical convolutions, *Nature Physics* **12**, 588 (2016).
- [9] E. Lejeune, A. Javili, J. Weickenmeier, E. Kuhl, and C. Linder, Tri-layer wrinkling as a mechanism for anchoring center initiation in the developing cerebellum, *Soft Matter* **12**, 5613 (2016).
- [10] E. Lejeune, B. Dortdivanlioglu, E. Kuhl, and C. Linder, Understanding the mechanical link between oriented cell division and cerebellar morphogenesis, *Soft Matter* **15**, 2204 (2019).
- [11] T. Engstrom, T. Zhang, A. Lawton, A. Joyner, and J. M. Schwarz, Buckling without bending: a new paradigm in morphogenesis, *Physical Review X* **8**, 041053 (2018).
- [12] A. K. Lawton, T. Engstrom, D. Rohrbach, M. Omura, D. H. Turnbull, J. Mamou, T. Zhang, J. M. Schwarz, and A. L. Joyner, Cerebellar folding is initiated by mechanical constraints on a fluid-like layer without a cellular pre-pattern, *Elife* **8**, e45019 (2019).
- [13] G. Xu, A. K. Knutsen, C. D. Dikranian, K. Kroenke, P. V. Bayly, and T. L. A., Axons pull on the brain, but tension does not drive cortical folding., *J. Biomech. Eng.* **132**, 071013 (2010).
- [14] M. A. Lancaster, M. Renner, C.-A. Martin, D. Wenzel, L. S. Bicknell, M. E. Hurles, T. Homfray, J. M. Penninger, A. P. Jackson, and J. A. Knoblich, Cerebral organoids model human brain development and microcephaly, *Nature* **501**, 373 (2013).
- [15] S. Benito-Kwiecinski, S. L. Giandomenico, M. Sutcliffe, E. S. Riis, P. Freire-Pritchett, I. Kelava, S. Wunderlich, U. Martin, G. A. Wray, K. McDole, and M. A. Lancaster, An early cell shape transition drives evolutionary expansion of the human forebrain, *Cell* **184**, 2084 (2021).
- [16] E. Karzbrun, A. Kshirsagar, S. R. Cohen, J. H. Hanna, and O. Reiner, Human brain organoids on a chip reveal the physics of folding, *Nature Physics* **14**, 515 (2018).
- [17] S. Velasco, A. J. Kedaigle, S. K. Simmons, A. Nash, M. Rocha, G. Quadrato, B. Paulsen, L. Nguyen, X. Adiconis, A. Regev, J. Z. Levin, and P. Arlotta, Individual brain organoids reproducibly form cell diversity of the human cerebral cortex, *Nature* **570**, 523 (2019).
- [18] C. A. Trujillo, R. Gao, P. D. Negraes, and et al., Complex oscillatory waves emerging from cortical organoids model early human brain network development, *Cell Stem Cell* **25**, 558 (2019).
- [19] G. Beaune, T. V. Stirbat, N. Khalifat, O. Cochet-Escartin, S. Garcia, V. V. Gurchenkov, M. P. Murrell, S. Dufour, D. Cuvelier, and F. Brochard-Wyart, How cells flow in the spreading of cellular aggregates, *Proceedings of the National Academy of Sciences* **111**, 8055 (2014), <https://www.pnas.org/content/111/22/8055.full.pdf>.
- [20] T. V. Stirbat, A. Mgharbel, S. Bodenec, K. Ferri, H. C. Mertani, J.-P. Rieu, and H. Delanoë-Ayari, Fine tuning of tissues' viscosity and surface tension through contractility suggests a new role for α -catenin, *PloS one* **8**, e52554 (2013).
- [21] K. Guevorkian, M.-J. Colbert, M. Durth, S. Dufour, and F. m. c. Brochard-Wyart, Aspiration of biological viscoelastic drops, *Phys. Rev. Lett.* **104**, 218101 (2010).
- [22] M. C. Gandikota and J. M. Schwarz, Buckling without bending morphogenesis: nonlinearities, spatial confinement, and branching hierarchies, *New J. Phys.* **23**, 063060 (2021).
- [23] A. Borzou, A. E. Patteson, and J. M. Schwarz, A Data-Driven Statistical Description for the Hydrodynamics of Active Matter, arXiv e-prints, arXiv:2103.03461 (2021), arXiv:2103.03461 [cond-mat.soft].
- [24] G. R. Martin and M. J. Evans, Differentiation of clonal lines of teratocarcinoma cells: Formation of embryoid bodies in vitro, *Proc. Natl. Acad. Sci. USA* **72**, 1441 (1975).
- [25] M. Murrell, P. Oakes, M. Lenz, and M. Gardel, Forcing cells into shapes: the mechanics of actomyosin contractility, *Nat. Rev. Mol. Cell Biol.* **16**, 486 (2015).
- [26] J. D. Humphrey, E. R. Dufresne, and M. A. Schwartz, Mechanotransduction and extracellular homeostasis, *Nat. Rev. Mol. Cell Biol.* **15**, 802 (2014).
- [27] P. Steinhardt, V. Mukhanov, V. Mukhanov, A. Linde, C. U. Press, and M. Viatcheslav, *Physical Foundations of Cosmology*, Physical Foundations of Cosmology (Cambridge University Press, 2005).
- [28] J. Binney and S. Tremaine, *Galactic Dynamics: Second Edition*, Princeton Series in Astrophysics (Princeton University Press, 2008).
- [29] H. Honda, Description of cellular patterns by dirichlet

domains: the two-dimensional case., J. Theor. Biol. **72**, 523 (1978).

- [30] S. Kaliman, C. Jayachandran, F. Rehfeldt, and A.-S. Smith, Limits of applicability of the voronoi tessellation determined by centers of cell nuclei to epithelium morphology, *Frontiers in Physiology* **7**, 551 (2016).
- [31] M. Versaevol, T. Grevesse, and S. Gabriele, Spatial coordination between cell and nuclear shape within micropatterned endothelial cells, *Nat. Commun.* **3**, 671 (2012).
- [32] H. G. Yevick, P. W. Miller, J. Dunkel, and A. C. Martin, Structural redundancy in supracellular actomyosin networks enables robust tissue folding, *Developmental Cell* **50**, 586 (2019).
- [33] A. M. Greiner, H. Chen, J. P. Spatz, and R. Kemkemer, Cyclic tensile strain controls cell shape and directs active stress fiber formation and focal adhesion alignment in spreading cells, *PLoS ONE* **8**, e77328 (2013).
- [34] A. S. G. Van Oosten, M. Vahabi, A. J. Licup, A. Sharma, P. A. Galie, F. C. MacKintosh, and P. A. Janmey, Uncoupling shear and uniaxial elastic moduli of semiflexible biopolymer networks: compression-softening and stretch-stiffening, *Sci. Reps.* **6**, 19270 (2016).
- [35] O. Larsell, *The Comparative Anatomy and Histology of the Cerebellum* (University of Minnesota Press, 1967).
- [36] A. Sudarov and A. L. Joyner, Cerebellum morphogenesis: the foliation pattern is orchestrated by multi-cellular anchoring centers, *Neural Development* **2**, 26 (2007).
- [37] A. Mongera and et al., A fluid-to-solid jamming transition underlies vertebrate body axis elongation, *Nature* **561**, 401 (2018).
- [38] A. Jain and et al, Regionalized tissue fluidization is required for epithelial gap closure during insect gastrulation, *Nature Communications* **11**, 5604 (2020).
- [39] S. Kim, M. Pochitaloff, G. A. Stooke-Vaughan, and O. Campas, Embryonic tissues as active foams, *Nature Phys.* **17**, 859 (2021).
- [40] R. Brandt, R. Rohlfing, J. Rybak, S. Krofczik, A. Maye, M. Westerhoff, H.-C. Hege, and R. Menzel, Three-dimensional average-shape atlas of the honeybee brain and its applications, *J. Comp. Neurol.* **492**, 1 (2005).
- [41] A. H. Guth and S. Y. Pi, Fluctuations in the New Inflationary Universe, *Phys. Rev. Lett.* **49**, 1110 (1982).
- [42] A. A. Starobinsky, Dynamics of phase transition in the new inflationary universe scenario and generation of perturbations, *Physics Letters B* **117**, 175 (1982).
- [43] S. W. Hawking, The development of irregularities in a single bubble inflationary universe, *Physics Letters B* **115**, 295 (1982).

Appendix A: Stage I analysis

The conventional approach to solving Eq. (1) is to compute its first two moments with respect to velocities leading to two differential equations for the number density

ρ , the bulk velocity \bar{v}^j , and $\overline{v^i v^j}$ each defined as

$$\begin{aligned}\rho &\equiv \int dv f, \\ \bar{v}^j &\equiv \frac{1}{\rho} \int dv v^j f, \\ \overline{v^i v^j} &\equiv \frac{1}{\rho} \int dv v^i v^j f\end{aligned}\quad (\text{A1})$$

such that

$$\begin{aligned}\frac{\partial \rho}{\partial t} + \partial_i (\rho \bar{v}^i) &= \int dv C, \\ \frac{\partial}{\partial t} (\rho \bar{v}^j) + \partial_i (\rho \overline{v^i v^j}) + \rho g^j &= \int dv C v^j.\end{aligned}\quad (\text{A2})$$

However, a common problem with this approach is that there are three unknown variables, but only two differential equations in Eq. (A2). One can find another differential equation for $\overline{v^i v^j}$, which would depend on higher moments of f . A common remedy is to assume a relationship between the number density and the pressure of the system. To do so, we define the stress tensor as

$$\sigma^{2ij} \equiv \overline{v^i v^j} - \bar{v}^i \bar{v}^j. \quad (\text{A3})$$

Since the system looks the same at different angles at least at the beginning stages, we assume that the stress tensor is isotropic and write $\sigma^{2ij} = \sigma^2 \delta^{ij}$. We then use data from the experiment movies reported in Ref. [16] and applied our data-driven method presented in Ref. [23] to find that the pressure of the cell nuclei linearly depends on the number density with a proportionality coefficient of $\sigma^2 = 0.1$ (see Appendix Fig. A1). With this finding, the final form of the evolution equation set reads

$$\begin{aligned}\partial_t \rho + \partial_i (\rho \bar{v}_i) &= C_0, \\ \partial_t \bar{v}_j + \sigma^2 \partial_j \rho + \bar{v}_i \partial_i \bar{v}_j + g_j &= \frac{1}{\rho} (C_j - \bar{v}_j C_0),\end{aligned}\quad (\text{A4})$$

where $C_0 \equiv \int dv C$, which account for cell division and the noise, and $C_j \equiv \int dv C v_j$, which accounts for dissipation and noise. More details regarding C_0 and C_j are discussed in the main section of the manuscript. The evolution equations are then solved in the linear regime after which time the final condition for the linear regime is then used as an initial condition for the nonlinear regime.

1. Linear evolution

In the linear regime, we assume that the number density is initially homogeneous with some small fluctuations, or

$$\rho \equiv \rho_0 + \delta\rho, \quad (\text{A5})$$

with $\delta\rho \ll \rho_0$. Inserting this equation into Eqs. (A4) and neglecting higher-order terms, they read

$$\begin{aligned}\frac{\partial}{\partial t} \delta\rho + \rho_0 \partial_i \bar{v}_i &= C_{0\text{noise}}, \\ \frac{\partial}{\partial t} \bar{v}_j + \sigma^2 \partial_j \delta\rho + (g_j - C_j/\rho_0) &= 0,\end{aligned}\quad (\text{A6})$$

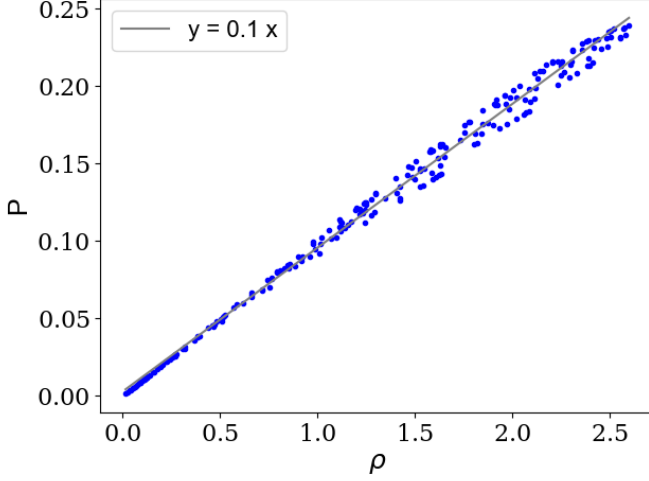


FIG. A1. Relationship between the pressure and cell nuclei density extracted from Supplementary Movie II from Ref. [16] using the data-driven technique presented in Ref. [23].

where we have neglected \bar{v}^2 and $C_{0\text{noise}}\bar{v}$ since they are of the order of $\mathcal{O}(\delta\rho^2)$. Moreover, we have assumed that the bulk velocity \bar{v}_i , the damping contribution to C_j , and the coefficient of the pressure σ^2 are all small and of the order of $\mathcal{O}(\delta\rho)$. The effects of damping are discussed in the next subsection.

To work towards a solution, we Fourier transform Eq. (A6) to arrive at

$$\begin{aligned} \partial_t \tilde{\delta} + ik_i \rho_0 \tilde{v}_i &= \tilde{C}_{0\text{noise}}, \\ \partial_t \tilde{v}_j + \sigma^2 ik_j \tilde{\delta} + \tilde{g}_j &= \tilde{C}_{j\text{noise}}/\rho_0, \end{aligned} \quad (\text{A7})$$

where $\tilde{\delta}$, \tilde{v} , and \tilde{g}_j refer to the k mode of the Fourier transformations of $\delta\rho$, \bar{v} , and $g_j - C_{j\text{no-noise}}/\rho_0$ respectively. Also, $\tilde{C}_{0\text{noise}}$ and $\tilde{C}_{j\text{noise}}$ denote the Fourier transformation of the respective noise contributions and obey $\langle \tilde{C}_{0\text{noise}} \rangle = \langle \tilde{C}_{j\text{noise}} \rangle = 0$, along with

$$\begin{aligned} \langle \tilde{C}_{0\text{noise}} \tilde{C}_{0\text{noise}} \rangle &= (2\pi)^3 \theta\delta(t-t')\delta^3(\vec{k} + \vec{k}'), \\ \langle \tilde{C}_{i\text{noise}}(t, \vec{k}) \tilde{C}_{j\text{noise}}(t', \vec{k}') \rangle &= (2\pi)^3 \gamma \times \\ &\delta_{ij} \delta(t-t')\delta^3(\vec{k} + \vec{k}'). \end{aligned} \quad (\text{A8})$$

With this form for the noise, the variables are functions of the same mode k , i.e. mode k' and k are independent. To proceed, we assume that

$$\tilde{g}_j = -ik_j \mathcal{L}^{-1} \tilde{\delta}. \quad (\text{A9})$$

As discussed in the main text, we choose a specific form $\mathcal{L}^{-\infty}$ and continue with the formal solution for the evolution of initial overdensities. We define $\tilde{X} \equiv ik_i \tilde{v}_i$ and multiply the second line of Eq. (A7) by ik_j to write the set of equations as

$$\begin{aligned} \partial_t \tilde{\delta} + \rho_0 \tilde{X} &= \tilde{C}_{0\text{noise}}, \\ \partial_t \tilde{X} + k^2 (\mathcal{L}^{-1} - \sigma^2) \tilde{\delta} &= ik_j \tilde{C}_{j\text{noise}}/\rho_0, \end{aligned} \quad (\text{A10})$$

which can be written in the following matrix form

$$\partial_t \begin{pmatrix} \tilde{\delta} \\ \tilde{X} \end{pmatrix} + M \cdot \begin{pmatrix} \tilde{\delta} \\ \tilde{X} \end{pmatrix} = \begin{pmatrix} \text{noise} \\ \text{noise} \end{pmatrix}, \quad (\text{A11})$$

where

$$\hat{M} = \begin{pmatrix} 0 & \rho_0 \\ k^2 (\mathcal{L}^{-1} - \sigma^2) & 0 \end{pmatrix}. \quad (\text{A12})$$

To solve Eq. (A11), we decouple the two equations by diagonalizing matrix \hat{M} with matrix \hat{U}^{-1} and rewrite it in the following form

$$\partial_t \tilde{Y} + \hat{M}_d \cdot \tilde{Y} = \begin{pmatrix} \text{noise}' \\ \text{noise}' \end{pmatrix}, \quad (\text{A13})$$

where

$$\begin{aligned} \tilde{Y} &= U^{-1} \cdot \begin{pmatrix} \tilde{\delta} \\ \tilde{X} \end{pmatrix}, \\ M_d &= U^{-1} \cdot M \cdot U. \end{aligned} \quad (\text{A14})$$

The prime on the noise means it is transformed by the U^{-1} matrix as well. We define U such that M_d is a diagonal matrix. Therefore, the solution to each component of Y reads

$$\begin{aligned} \tilde{Y}_i &= \tilde{Y}_i(t=0) \exp(-M_{d_{ii}} t) \\ &+ \text{noise}'_i (1 - \exp(-M_{d_{ii}} t)). \end{aligned} \quad (\text{A15})$$

This equation indicates that the noise is irrelevant for the modes that grow over time and become seeds for the large-scale structures in the non-linear regime. The reason is that the growing modes are those in which $M_{d_{ii}}$ is negative and for these modes the noise term in right hand side of the equation becomes rapidly negligible. It should be noted that the linear regime is only valid until $\tilde{Y} < 1$ and the noise term will not appear with a negative coefficient at $t \gg 0$. Interestingly, the same exponentially growing modes are the seeds to the galaxies in the cosmos. Finally, the solutions to the variables of interest are

$$\begin{pmatrix} \tilde{\delta}(t, \vec{k}) \\ \tilde{X}(t, \vec{k}) \end{pmatrix} = U \cdot \begin{pmatrix} \tilde{Y}_1 \\ \tilde{Y}_2 \end{pmatrix}. \quad (\text{A16})$$

At this point, we have solved the differential equations in Fourier space and now convert back to configuration space where the solution reads

$$\delta\rho(t, \vec{x}) = \int d^3k e^{i\vec{k}\cdot\vec{x}} \tilde{\delta}(t, \vec{k}), \quad (\text{A17})$$

where

$$\tilde{\delta}(t, \vec{k}) = \tilde{\delta}(t=0, \vec{k}) \cosh\left(\sqrt{\rho_0(\mathcal{L}^{-1} - \sigma^2)} kt\right) \quad (\text{A18})$$

Since \mathcal{L}^{-1} is also a function of k , for some modes the square root takes imaginary values, leading to oscillations, which we do not focus on here. This model

can readily be tested against observations. An interesting set of observable quantities in the linear regime is the time-evolved correlations between the overdensities $\langle \delta\rho(t, x_1) \cdots \delta\rho(t, x_n) \rangle$. Therefore, one can determine the form of \mathcal{L}^{-1} using a few of these correlation functions and further interrogate the model using the rest of the correlation functions.

a. The Effects of Dissipation

Here we study how a force proportional to the negative of velocity, to model dissipation, affects the structure formation in the linear regime. Therefore, we replace $C_j \rightarrow C_j - a_2\rho_0\bar{v}_j$

$$\begin{aligned} \frac{\partial}{\partial t}\delta\rho + \rho_0\partial_i\bar{v}_i &= 0, \\ \frac{\partial}{\partial t}\bar{v}_j + \sigma^2\partial_j\delta\rho + (g_j - C_j/\rho_0) + a_2\bar{v}_j &= 0, \end{aligned} \quad (\text{A19})$$

which in momentum space reads

$$\begin{aligned} \partial_t\tilde{\delta} + \rho_0\tilde{X} &= 0, \\ \partial_t\tilde{X} + k^2(\mathcal{L}^{-1} - \sigma^2)\tilde{\delta} + a_2\tilde{X} &= 0. \end{aligned} \quad (\text{A20})$$

This coupled system of equations can then be written in the following matrix form

$$\partial_t \begin{pmatrix} \tilde{\delta} \\ \tilde{X} \end{pmatrix} + M \cdot \begin{pmatrix} \tilde{\delta} \\ \tilde{X} \end{pmatrix} = 0, \quad (\text{A21})$$

where

$$M = \begin{pmatrix} 0 & \rho_0 \\ k^2(\mathcal{L}^{-1} - \sigma^2) & a_2 \end{pmatrix}. \quad (\text{A22})$$

Then

$$\tilde{\delta}(t, \vec{k}) = \tilde{\delta}(t=0, \vec{k})e^{-\frac{a_2 t}{2}}(A+B), \quad (\text{A23})$$

with

$$\begin{aligned} A &\equiv \cosh\left(\frac{1}{2}t\sqrt{4k^2\rho_0(\mathcal{L}^{-1} - \sigma^2) + a_2^2}\right), \\ B &\equiv \frac{a_2 \sinh\left(\frac{1}{2}t\sqrt{4k^2\rho_0(\mathcal{L}^{-1} - \sigma^2) + a_2^2}\right)}{\sqrt{4k^2\rho_0(\mathcal{L}^{-1} - \sigma^2) + a_2^2}}. \end{aligned} \quad (\text{A24})$$

Fourier transforming back to configuration space, we integrate over k -modes from zero to infinity. For some large k , $4k^2\rho_0(\mathcal{L}^{-1} - \sigma^2) \gg a_2^2$ at short times,

$$\tilde{\delta}(t, \vec{k}) \simeq \tilde{\delta}(t=0, \vec{k}) \exp\left(tk\sqrt{\rho_0(\mathcal{L}^{-1} - \sigma^2)}\right). \quad (\text{A25})$$

On the other hand, for small k -modes where $4k^2\rho_0(\mathcal{L}^{-1} - \sigma^2) \ll a_2^2$, the over-densities will dissolve after some time since

$$\tilde{\delta}(t, \vec{k}) \propto \tilde{\delta}(t=0, \vec{k}) \exp\left(-\frac{a_2 t}{2}\right). \quad (\text{A26})$$

In sum, dissipation effects lead to removal of small k -modes, while larger k -modes still grow over time and create seeds for the non-linear regime. Observation of the smallest scales that form in the experiment can be used to set the dissipation effects using data.

2. Non-linear evolution

We now study the non-linear regime of the large-scale structure formation. We reset $t=0$ to the beginning of the non-linear regime. At the end of the linear era we have

$$\begin{aligned} \rho &\simeq \rho_0, \\ \partial_t\rho &\simeq 0, \\ \bar{v}_r &= -v_0, \end{aligned} \quad (\text{A27})$$

where in the first line we have used $\delta\rho \ll \rho_0$. Also, $v_0 > 0$ is the magnitude of the bulk velocity at the beginning of the non-linear regime. Since the cortex-core structures in the brain organoid are nearly spherically symmetric, we write the closed system of differential equations as

$$\begin{aligned} \frac{\partial\rho}{\partial t} + \frac{2}{r}\rho\bar{v}_r + \partial_r(\rho\bar{v}_r) &= C_0, \\ \frac{\partial}{\partial t}\bar{v}_r + \sigma^2\partial_r\rho + \bar{v}_r\partial_r\bar{v}_r + g_r &= \frac{1}{\rho}C_r, \end{aligned} \quad (\text{A28})$$

where we have used the isotropic assumption to infer that in the spherical coordinate system $\vec{v} = (\bar{v}_r, 0)$. We use the first differential equation in the exact evolution set in Eq. (A28) to eliminate the bulk velocity in terms of the number density

$$\bar{v}_r(t, r) = -\frac{1}{r^2\rho(t, r)} \int dr r^2 \partial_t\rho(t, r) + \frac{A(t)}{r^2\rho(t, r)} \quad (\text{A29})$$

where $A(t)$ is an arbitrary function of time. Since the values of the number density and the bulk velocity at the end of the linear regime serve as the initial conditions for the non-linear regime, the rest of the initial conditions are given in Eq. (A27). Moreover, at the end of the cortex-core formation, the system satisfies the conditions

$$\begin{aligned} \rho &\rightarrow F(r), \\ A &\rightarrow 0, \\ \bar{v}_r &\rightarrow 0, \end{aligned} \quad (\text{A30})$$

where $F(r)$ is the form of the cell nuclei number density that can be observed at around Day 3 of the experiment [16] and fit it to a polynomial function. The fit is plotted in Fig. A3.

Let us address the number of unknown variables and the means of determining them. Unlike in cosmology, the forces in the brain organoid system may evolve in time due to restructuring of the cellular cytoskeleton in response to the extracellular environment, for instance. In the linear regime, we assumed a minimal form for the interaction between similar cell nuclei. As the

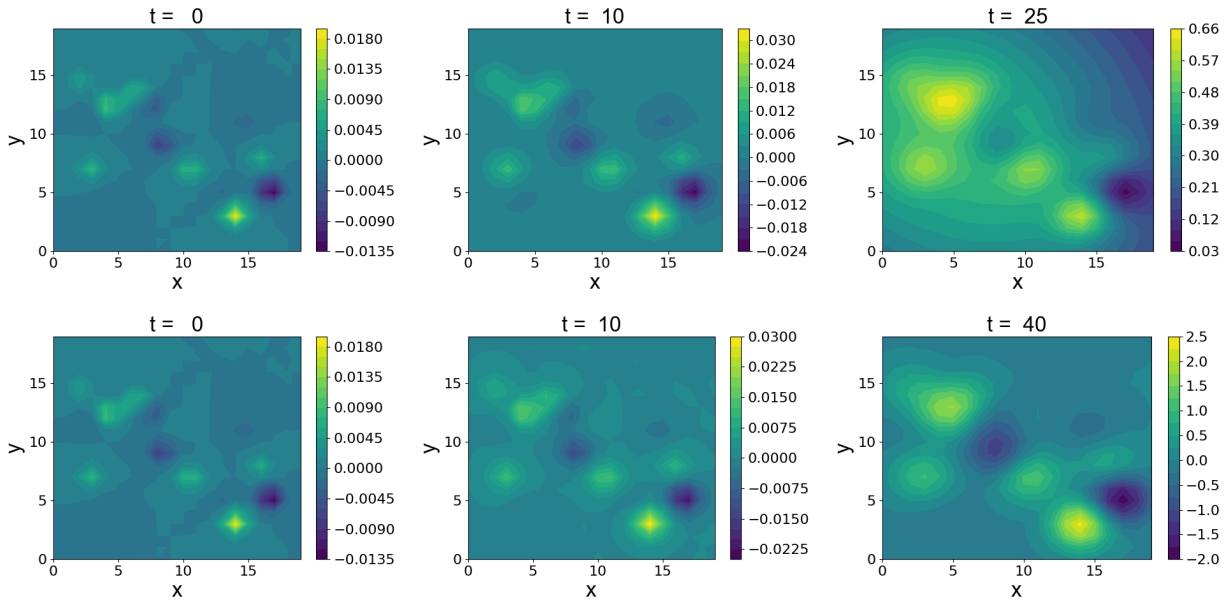


FIG. A2. Top row: The time evolution for $\delta\rho$ as a function of positions x and y for $\mathcal{L}^{-1} = \frac{1}{k^2+0.12} + \frac{0.1}{k^4+0.14}$. Bottom row: Same as top row but with $\mathcal{L}^{-1} = \frac{1}{k^2+0.12}$, just as in the Fig. 2 in the main text.

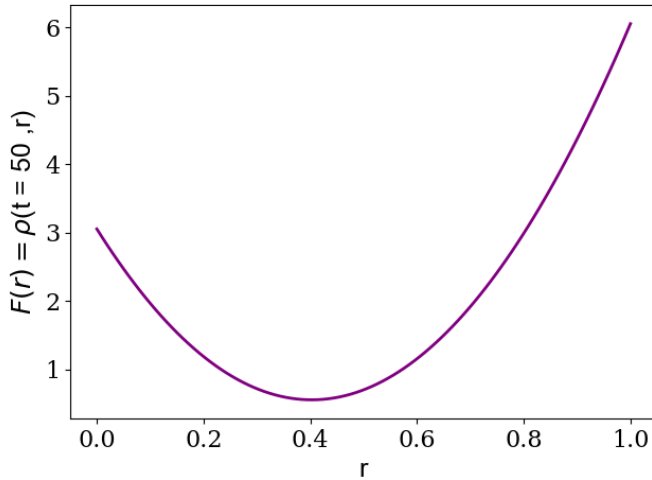


FIG. A3. The cell nuclei density $F(r)$ on Day 3 observed in the experiments in Ref [16].

brain organoid system evolves, the forces evolve. Hence, $g_r(t, r)$ should be considered unknown. In addition, the damping effects in $C_r(t, r)$ and $A(t)$ are also unknown. The number density $\rho(t, r)$ is another unknown variable. One of these unknowns can be found by solving the remaining equation in Eq. (A28). The rest should be found either through data, and whenever data is not available, by assumption or argument. Accordingly, we construct an analytic form for $\rho(t, r)$ and $A(t)$ using observations,

and solve the second line in Eq. (A28) to determine the time evolution for the net force on the cell nuclei, i.e. $g_r(t, r) - C_r(t, r)/\rho(t, r)$. We assume the number density to be represented by the following profile

$$\rho(t, r) = \rho_0 e^{-t/\tau} + F(r) (1 - e^{-t/\tau}), \quad (\text{A31})$$

where τ is the half-life of the experiment equivalent to 1.5 days. Moreover, given the initial and final conditions, we assume that $A(t) = 0$. We can now determine the time evolution of $\bar{v}_r(t, r)$ and $g_r(t, r) - C_r(t, r)/\rho(t, r)$. The results are shown in Fig. A3.

Now that we have computed the net force on any given cell nuclei, we ask what can we infer about nuclei shape. Assuming that the contractile forces are given by Eq. (A9) throughout the nonlinear regime, the net force of such interaction on a cell nuclei at position \vec{x} is given by

$$\vec{f}_{\text{cell-cell}}(\vec{x}) = i \int \frac{d^3 k}{(2\pi)^3} \vec{k} \mathcal{L}^{-1} \int d^3 x' \rho(\vec{x}') e^{i\vec{k} \cdot (\vec{x} - \vec{x}')} \quad (\text{A32})$$

The remaining contribution of net force on a cell nuclei is due to emergent interactions, either with other cells or with the extracellular environment. To obtain Fig. 3b, we insert $F(r)$ into the above equation, include first term of \mathcal{L}^{-1} in Eq. (10), set $b = 0.1$, and calculate the integral in Eq. A32. The result is shown in Fig. 3b. The difference between this latter force and the net force in Fig. 3b is the emergent force.